3D damage imaging of Carrara marble sculptures by acoustic tomography coupled to photogrammetry

Marie-Laure Chavazas, Jérémie Berthonneau, Cédric Payan, Éric Debieu, Philippe Bromblet

3D damage imaging of Carrara marble sculptures by acoustic tomography coupled to photogrammetry

Marie-Laure Chavazas[1, 2] *, Jérémie Berthonneau[2], Cédric Payan[1], Éric Debieu[1], Philippe Bromblet[2]

[1] Aix Marseille Univ, CNRS, Centrale Med, LMA UMR 7031, 4 impasse Nikola Tesla, Marseille, France

[2] Centre Interdisciplinaire de Conservation et de Restauration du Patrimoine, 21 rue Guibal, Marseille, France

* Corresponding author:
e-mail: marie-laure.chavazas@cicrp.fr
full postal address: Marie-Laure Chavazas CICRP 21, rue Guibal 13 003 Marseille France

E-mail addresses:
- Jérémie Berthonneau: jeremie.berthonneau@cicrp.fr
- Cédric Payan: cedric.payan@univ-amu.fr
- Éric Debieu: eric.debieu@cnrs.fr
- Philippe Bromblet: philippe.bromblet@cicrp.fr

Length of the manuscript (including references, tables and captions): 6927 words

Highlights

- 3D imaging of the mechanical state of two Roman Carrara marble sculptures
- Photogrammetric models projected instead of using markers for transducer positions
- Degradation state coincides with degree of exposure to weather conditions
- Better insight on conservation issues thanks to crack depth profile estimation

Abstract

Marble is known for its sensitivity to weathering. Therefore, marble sculptures can develop superficial and inner alterations when subjected to weather conditions. Addressing a complete condition report of these alterations is essential for defining the conservation conditions and planning restoration. However, while superficial alterations can be reported by simple visual inspections, the identification of inner defects necessitate more complex inspection methods. Besides, the evaluation of the conservation state of cultural heritage artefacts requires the use of non-destructive techniques. This research thus aims at investigating the influence of exposure to weather conditions on the degradation state of two Carrara marble sculptures from the Roman theater of Arles, France, as well as at answering specific conservation issues coming from curators. To do so, acoustic tomography coupled to photogrammetry was carried out to document the superficial state as well as to probe the inner state of the objects under study. A new method is tested to locate the transducer positions (without any sticky material): the 3D photogrammetric models of the sculptures were projected directly onto them to mark the transducer positions immediately on the model. The 3D models were then used to measure the distances between each emitter and receiver position. This approach also allows saving the transducer positions on the 3D model, which provides a digital record of measurement positions in case of additional future measurements. Overall, the degradation state of the sculptures studied coincides with their degree of exposure to weather conditions during Roman times, highlighting marble sensitivity to climatic conditions. Besides, depth profiles were estimated for visible cracks with the time-of-flight diffraction method and showed that the most worrying crack had not propagated inside the sculpture as much as curators feared, pointing out that acoustic techniques can be support tools for conservators.

Keywords: damage imaging, acoustic tomography, photogrammetry, stone cultural heritage

1. Introduction

Marble sculptures can develop various superficial or inner alterations over time due to their conservation history [1]. When exposed outdoors, marble is known for its sensitivity to climatic conditions. Marini and Bellopede (2007) showed that marble slabs sheltered for climatic conditions exhibited less bowing than those fully subjected to weather conditions [2]. Some studies also showed a residual dilatation of marble samples during the first thermal cycle up to 80 – 90 °C [3,4]. Malaga et al. (2002) observed from porosity measurements an initiation of granular decohesion at 40 – 50 °C [5]. Besides, previous works showed that residual strain during thermal cycling is more pronounced in presence of moisture than in a dry environment [4,6–8]. Moreover, the latest studies have shown a measurable thermal damage in Carrara marble for temperatures as low as 40 °C and a great impact of relative humidity level at marble microstructure level [9,10]. Thus, when considering ancient sculptures, it is necessary to keep in mind that internal defects or weak areas could be present within some parts of the object, depending on its exposure to weathering conditions. Conservators and curators would like to have a relevant non-destructive technique able to determine these non-visible defects. Our research aims to develop a new methodology coupling acoustic tomography to photogrammetry to obtain 3D damage imaging and to test it by investigating the internal conservation state of two marble sculptures which had different degrees of exposure to weather conditions in the Roman theater of Arles (France).

Acoustic methods enable mechanical properties to be non-destructively probed, even in the volume of an object. Therefore, these techniques are particularly well-adapted to evaluate the inner degradation state of marble sculptures. Among acoustic techniques, acoustic tomography allows reconstructing and mapping wave propagation velocity through a sculpture section or volume. Propagation velocity of longitudinal waves in marble has been linked to marble condition according to five damage classes [11,12]. The defined classes range from class 0 for velocities above 5,000 m/s corresponding to a fresh marble to class IV for velocities below 1,500 m/s corresponding to a crumbling one. 2D imaging of propagation velocity only gives information about plane surfaces of wall or slab, or about some cross sections in sculptures [13–19]. 3D imaging of propagation velocity can be even more interesting for diagnosis as it allows reconstructing the mechanical degradation state in the whole volume of the sculpted object of interest [16,20–25]. Thus, potential areas of weakness can be located at the global scale of the sculpture and not only in some cross sections. 2D and 3D imaging of propagation velocity are sometimes combined and compared to other methods such as ground-penetrating radar, infrared thermography, microstructural characterization [14–18,23]. The aim of acoustic tomography is generally to evaluate the global mechanical state of a sculpture and it can also be used to investigate the extent of superficial fractures [14,20], the structural efficiency of past restoration [18], or the sculpture history [23]. Acoustic tomography has successfully linked low velocity zones to visible superficial features, such as open cracks, mortar-filled fractures or junctions, in various studies on stone cultural heritage artefacts [14–18,20–23].

One of the difficulties in performing acoustic tomography on sculptures is the accurate measurement of distances between transducers. Indeed, sculptures have complex geometries which make it uneasy to use rule, tape measure or compass for precise distance measurements. Instead, 3D photogrammetric (or lasergrammetric) models can be employed [20–23,26]. The 3D photogrammetric model provides a digital replica of the sculpture, in terms of geometry and texture. The use of 3D photogrammetric model coupled to acoustic tomography enables greater efficiency during the measurement campaign as the transducer positions can be selected prior to the *in situ* measurements, accurate evaluation of the emitter-receiver distances during data processing, and a digital record of the measurement campaign that can be reused in the future for additional measurements. Such an approach has been previously used, not only in the cultural heritage field [27,28], but the way of locating the transducers on the 3D models involved the use of markers sticked on the sculptures surfaces [20–24,26]. However, such an invasive methodology does not meet the conditions of work generally imposed by curators to preserve the sculptures. Thus, to tackle both objectives of evaluating the inner cohesion of two sculptures while meeting conservation requirements, the present work proposes a fully non-destructive and non-invasive approach for 3D damage imaging of marble sculptures, by coupling acoustic tomography and photogrammetry and by projecting the 3D models onto the sculptures to directly locate the measurement points on the projections.

2. Research aim

Two Carrara marble sculptures with different degrees of exposure to weather conditions in Roman times were studied. Marble being particularly sensitive to climatic variations, the different degrees of exposure could have induced different degradation states in each sculpture. To evaluate sculpture conservation state, acoustic tomography was coupled to photogrammetry. Moreover, in this work, a new methodology was set up to optimize the distance measurements by locating measurement point positions on the projection of the 3D photogrammetric models onto the sculptures, instead of using markers as it has been usually done in previous studies.

3. Materials and methods

3.1.Studied sculptures

The Roman theater of Arles was built at the end of the 1st century BC, under Augustus reign (27 BC – 14 AD) [29]. A model of the theater during Roman times is shown in Fig. 1 (a). Today, the remains of the theater (Fig. 1 (b)) comprise the *cavea* (no. 1 in Fig. 1), the *orchestra* (no. 2 in Fig. 1) and some columns or column parts from the *scaenae frons* (no. 3 in Fig. 1). Besides, sculptures that were part of the monumental ornamentation of the theater are nowadays displayed in the Departmental Museum of Ancient Arles.

Two of these sculptures were studied in this work. Both date from the end of the 1st century BC and are made of Carrara marble [29]. One is an altar devoted to the god Apollo (Fig. 1 (c)), the other is a statue representing the Emperor Augustus (Fig. 1 (d)). Both sculptures were exposed outdoors in the Roman theater for several centuries until its destruction in the 5th century. The average weather data for Arles from 1980 to 2016 are as follows: the lowest average temperature fluctuates between 4 and 19 °C, the highest average temperature between 11 and 30 °C, the weather is mainly clear, the main wind direction is north [30]. However, the Roman theater was an almost closed place, thus winds should not have played as important a role as they do now.

The sculptures were located in different parts of the theater, as indicated in Fig. 1 (a) (in blue for the altar, in orange for the statue). Both sculptures were facing east in Roman times. The Apollo altar, provided with a base and topped by a pediment which has now disappeared, was put on the ground against the wall of the *pulpitum* (small wall supporting the front of the stage, no. 4 in Fig. 1). The back was almost not visible but the front was wholly exposed to weathering. The Augustus statue was partially protected in a niche in the *scaenae frons* (three-level wall behind the scene, no. 3 in Fig. 1) and undoubtedly by an awning which protected the scene from bad weather. Therefore, the statue was less exposed to weather conditions than the altar. The different exposures of the sculptures to weather conditions could have impacted their degradation state.

The Apollo altar was discovered during archaeological digs in 1823 and measures about 150 cm in length, 60 cm in width and 95 cm in height [29,31]. On the front side (Fig. 1 (c)), Apollo is represented with a lyre under his left arm and a Delphic tripod behind him. Two jambs are each decorated with a laurel, a tree dedicated to Apollo. The lateral sides of the altar (not displayed here) represent the punishment of Marsyas. The back, which was not visible in Roman times, had not been sculpted and has a smooth surface. At the top surface, two cracks are located at the interfaces between the middle and the lateral parts of the altar (Fig. 1 (e, f)). They go through its entire width and emerge at the front side on a length of about 20 cm. The right-side crack also emerges at the back on a length of 12 cm. The depths of the cracks inside the altar are yet unknown. The curators are particularly worried about the extent of the right-side crack, fearing that this part could break away from the rest of the altar. The

artwork is considered very fragile and not moveable, therefore any loan request for exhibition is refused. Thus, a better knowledge on the right-side crack depth would be very helpful for the curators.

The Augustus statue, displayed in Fig. 1 (d), was originally a sculpture from head to feet. Today, the only remaining parts are Augustus' head (excavated in 1834) and chest (excavated in 1750), both made of Carrara marble, and the drapery (excavated in 1834), made of limestone from the Bois de Lens (Nîmes area, France) [29,31]. The total height of the current statue is of 2.40 m [31]. The Augustus statue exhibits a thick circling vein on the chest and cracks along the vertical direction that seem to be very superficial from visual inspection. The vein and the cracks are indicated in Fig. 1 (g) by red and white arrows, respectively. The statue visually seems less deteriorated than the altar, which could be the first indication of a better conservation of the statue and coincides with its lower degree of exposure to weather conditions in the theater.

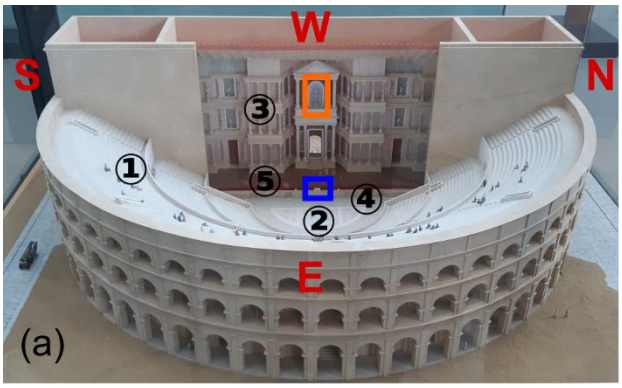
W
S
N
E
(a)

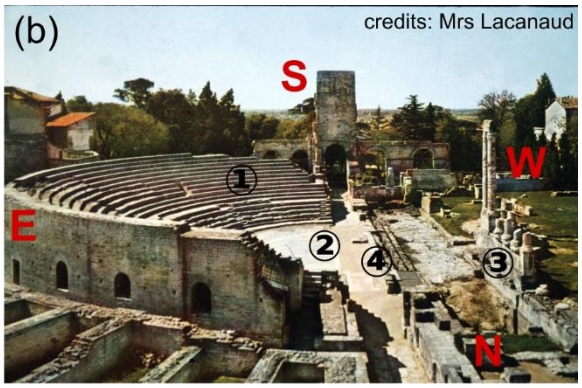
(b)
credits: Mrs Lacanaud
S
W
E
N


(c)


(d)


(e)


(f)

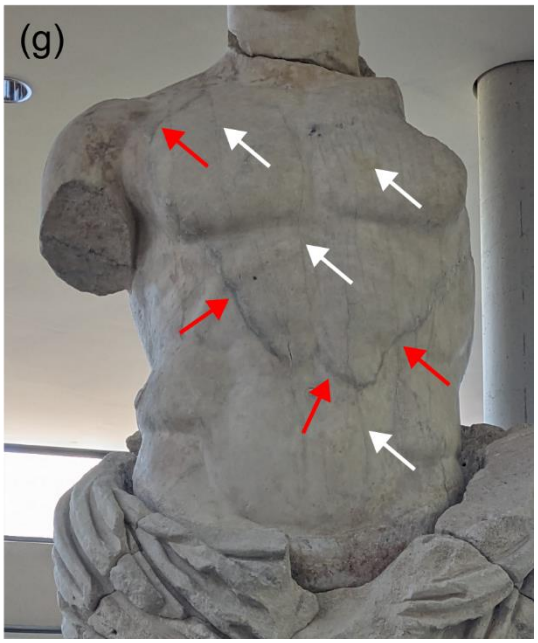
(g)

Fig. 1 (Color online) Presentation of the Roman theater and of the sculptures. (a) Model (Departmental Museum of Ancient Arles) and (b) remains of the Roman theater of Arles. (1) *Cavea*, (2) *orchestra*, (3) *scaenae frons*, (4) *pulpitum*, (5) wooden scene. Cardinal directions are indicated in red. The locations of the altar and the statue are indicated by blue and orange boxes, respectively. (c) Apollo altar. (d) Augustus statue. (e) Left-side and (f) right-side cracks on the altar indicated between white arrows. (g) Cracks (indicated by white arrows) and vein (indicated by red arrows) on the statue.

3.2.Acoustic tomography

Acoustic tomography allows imaging the inner structure of an object by probing variations of its mechanical properties. Here, travel-time tomography is used to estimate the variations of the apparent propagation velocity of longitudinal waves inside the sculptures. Propagation velocity V_P of longitudinal waves is directly linked to elastic characteristics such as Young's modulus E or Poisson's ratio υ: $E = \rho V_P^2$ (approximation for 1D geometries), with ρ the material density, and $\upsilon = (V_P^2 - 2\,V_S^2)/(2\,V_P^2 - 2\,V_S^2)$, with V_S the propagation velocity of shear waves. The propagation velocity of longitudinal waves is also positively correlated with uniaxial compressive, tensile, and flexural strength in various rock types [13,32]. Besides, wave propagation is influenced by the inner features of the studied object: the presence of microcracked areas, a fracture, a defect or a fractured area on the ultrasound path will lengthen their times of flight, causing a decrease of apparent propagation velocity. Material anisotropy and intrinsic inhomogeneities may also impact ultrasound propagation. Nevertheless, Carrara marble is a homogenous and almost isotropic material, therefore wave propagation velocities can be compared in every direction [11,33].

The times of flight were measured with a Proceq Pundit PL 200 device combined with flat Proceq transducers of 54 kHz which have a diameter of about 4 cm. The geometry of the transducers restricted the possible positions for the measuring points, particularly in the Apollo altar which features many reliefs, as the transducers had to be placed on rather flat surfaces. The travel times were manually picked on the apparatus screen by the same operator to ensure consistency. Ultrasonic gel could not be employed for ultrasound transmission between the transducers and the sculptures since the use of such gel could produce permanent stains on marble surface. Instead, supple polymer films and membranes were used to improve contact between the transducers and the surface and to protect the sculptures from direct contact with the metal transducers. Olympus polymer membranes were used between each transducer and the Augustus statue and between the receiver and the Apollo altar, and Melinex® was used between the emitter and the altar. The corresponding interfaces were included right from the calibration of the device which consists in measuring the difference between the theoretical and measured times of flight on a calibration rod to then transfer it to the measurements.

Given the complex geometries of the studied sculptures, the distances between the ultrasonic emitter and receiver were measured thanks to 3D photogrammetric models. The transducer positions were not indicated by markers sticked on the sculpted objects, as it has usually been done in similar studies [20–23]. Instead, the 3D models were projected directly onto the sculpture to instantaneously locate the emitter and receiver positions. The projection is illustrated in Fig. 2. The 3D photogrammetric models of both sculptures had been already acquired by the Departmental Museum of Ancient Arles and were kindly provided by the curators for this work [34]. During the measurement campaigns, the projection allowed replacing the emitter and the receiver back to the same position as measurement progressed since their positions were saved and marked by points on the 3D models. During the data processing, the saved positions were used to measure distances between emitters and receivers. Therefore, the direct projection of a 3D model is an interesting methodological improvement for i) directly locating transducers on the 3D model (no need to take new pictures to locate measurement points on the model afterward); ii) avoiding gluing markers on the object with potential contamination of the surface; and iii) time saving that can be useful to meet museum opening constrains.

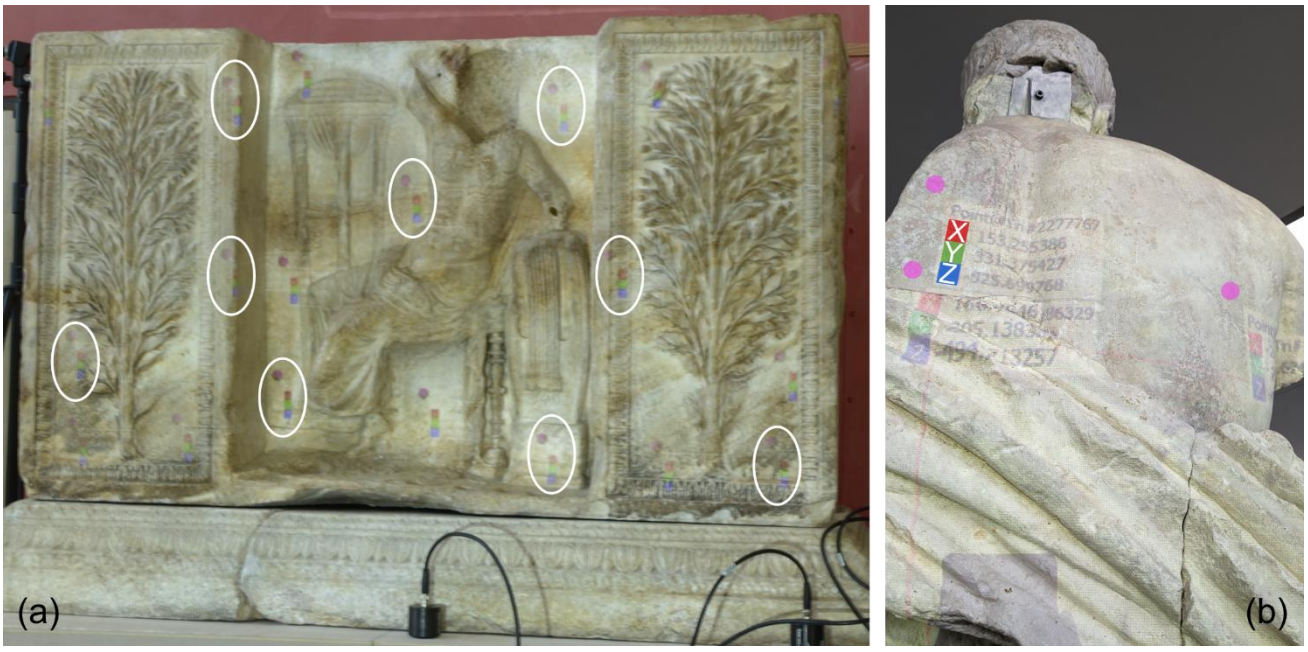

Fig. 2 (Color online) 3D model projection. The 3D models projected on (a) the Apollo altar and (b) the Augustus statue. Transducer positions are associated with their location (pink circles) and their 3D coordinates (red, green and blue squares). Some groups of location and coordinates are circled in white on the Apollo altar. On the back of the Augustus statue, the locations have been redrawn, as well as one group of coordinates, in order for them to stand out on the picture.

Nonetheless, the 3D model could not be projected at the back of the Apollo altar due to the presence of a chair rail behind it. Therefore, the emitter positions at the back of the altar were located with a black marker on a transparent Melinex® sheet and they were later reported on the 3D model. One projector was used to project the 3D model on the altar front side. 38 positions were defined for the emitter and 36 for the receiver on the Apollo altar, for a total of 552 time-of-flight measurements. For the Augustus statue, two projectors were used simultaneously to project the model on the two opposite sides of the statue. Only Augustus' chest was probed with acoustic tomography. Here, 21 positions were defined for the emitter and 20 for the receiver on the Augustus statue. In total, 270 time-of-flight measurements were made through Augustus' chest. All the positions of the emitter and the receiver on the sculptures can be found in the Supplementary Material.

The reconstruction of the local propagation velocities from the global times of flight was managed with a simultaneous iterative reconstruction technique (SIRT) [35]. SIRT is a procedure for solving linear equation systems. Here, the system is made of the vectors of global times of flight, and of the vector of local velocities (unknown) and of the matrix of travelled distances in each voxel into which the sculptures are virtually discretized. Voxel edges equal to half the wavelength (3 cm for both objects, with the frequency equal to 54 kHz and the propagation velocity equal to the average apparent velocity, i.e. 2.9 km/s for the altar and 3.6 km/s for the statue). Voxels having no ray coverage were then not considered at the inversion step. A straight-ray tracing was assumed to calculate apparent velocities, compute ray paths and calculate their travelled distance in each voxel. The reconstruction with SIRT was managed thanks to the Air Tools II Matlab package [35,36]. SIRT considers the equations on all the rays simultaneously at each iteration to solve the system and the component averaging (CAV) method was used. Result visualization and data integration in the 3D models was also managed in Matlab with functions by Bernard Abayowa and by Alutsyah Luthfian (readObj, display_obj, dispObj) [37–39].

3.3.Crack depth measurement

Depths of the Apollo altar cracks were estimated independently of the acoustic tomography, with another ultrasonic technique applicable to outcropping or surface cracks. The Proceq Pundit PL 200

device and two flat 54 kHz transducers were again used. The time-of-flight diffraction (TOFD) method is illustrated in Fig. 3 and consists in measuring times of flight between a fixed emitter (E) and a receiver (R) placed on a line crossing the crack at increasing distances from the emitter, before and after the crack. The relationship between time of flight and emitter – receiver distance can be fitted by a linear law (green curve in Fig. 3) when the receiver is placed before the crack, and by a polynomial law (orange curve in Fig. 3) when the receiver is placed beyond the crack [40,41]. The crack depth *h*, perpendicular to the surface, is then estimated by the following equation:

$$h = \frac{L}{2}\left(\frac{T_2}{T_1} - \frac{T_1}{T_2}\right) \quad (1)$$

where L is the distance between the emitter and the crack, T_1 and T_2 are the times of flight obtained at the crack position L from the linear and polynomial fits. Here, the depths of the altar cracks (Fig. 1 (e, f)) were evaluated with this method at different points along the cracks to estimate the crack profiles in the altar volume. It can be assumed that this method allows crack depth detection for depths above the diffraction limit which is of approximately 3 cm in this case $\left(\frac{\lambda}{2} = \frac{2924\ m/s}{2*54\ kHz}\right)$.

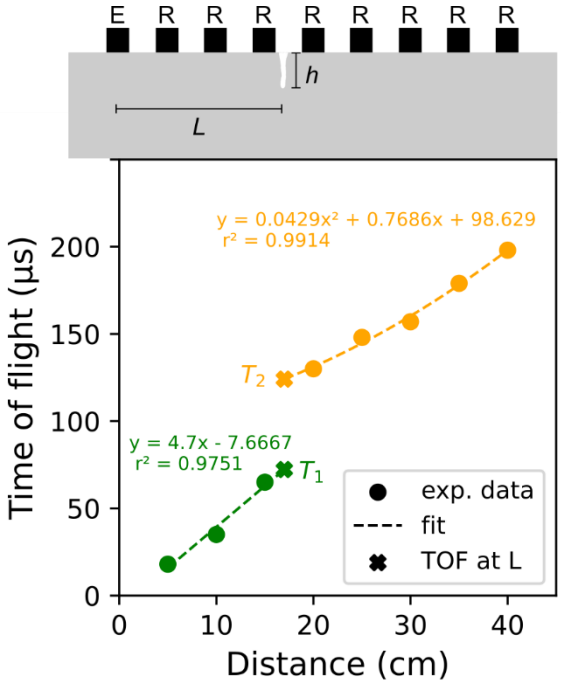

Fig. 3 (Color online) Explanatory scheme of the time-of-flight diffraction (TOFD) method. E denotes the emitter position and R the receiver positions. The crack depth *h* is estimated from the times of flight T_1 and T_2 obtained at the crack position L (here, L = 17 cm) from the linear and polynomial fits, respectively before and after the crack. Here, a depth *h* of 10 cm may be deduced.

4. Results

4.1. 3D imaging of propagation velocity

The results of apparent propagation velocity and of 3D imaging of propagation velocity are presented for the Apollo altar in Fig. 4 and for the Augustus statue in Fig. 5. In the results of apparent propagation

velocity (Fig. 4 (a) and Fig. 5 (a)), every emitter – receiver path is colored according to marble damage classes (Table 1) defined by Köhler [12]. The distribution of apparent propagation velocities are also presented in Fig. 4 (b) and Fig. 5 (b). The measurement precision on individual propagation velocities was experimentally determined to be of ±10%. In the results of 3D velocity imaging (Fig. 4 (c) and Fig. 5 (c)), the velocities reconstructed by SIRT are interpolated and visualized on cartographies sliced along planes. Anomalous velocities were deleted so that velocity variations are readable on the cartographies. An upper limit of 7.0 km/s was chosen for the plotted velocities. Voxels with velocity values above this limit correspond to 0.6% and 0.8% of total voxels associated with a velocity value, respectively for the altar and the statue. Therefore, most of the reconstructed velocities lie in a physically realistic range. Histograms of the reconstructed velocities can also be found in the Supplementary Material. Moreover, tables classifying propagation velocities from different sculpture parts by damage classes can also be found in the Supplementary Material.

The average apparent and reconstructed velocity values in the Apollo altar are in very good agreement: 2.9 ± 0.5 km/s and 2.9 ± 0.6 km/s, respectively. This average value corresponds to the upper limit of damage class II. Apparent velocities measured in the altar belong to damage class from I (light green lines in Fig. 4 (a)) to III (red lines in Fig. 4 (a)). 3% of total measured apparent propagation velocities belong to damage class III. The analysis of the 3D velocity image slices for the Apollo altar indicates weakest zones at the back of the altar. This is confirmed statistically as 57% of velocities from damage classes III and IV are situated in the last 15 cm of the altar back which represents 41% of the reconstructed volume of the altar.

The average apparent and reconstructed velocities are also in agreement in Augustus' chest: 3.6 ± 0.6 km/s and 3.7 ± 0.6 km/s, respectively. Both values correspond to damage class I. The apparent velocities measured in the statue belong to damage class from 0 (dark green lines in Fig. 5 (a)) to II (orange lines in Fig. 5 (a)). The 3D velocity image shows that the upper part of Augustus' chest seems to contain more low velocity values than the lower part (Fig. 5 (b, c)). Velocity counting shows that indeed the upper half of the chest (57% of the reconstructed volume) comprises less class 0 velocities (44%) and more class II velocities (75%) than the lower half. Besides, more velocities from classes II and III (22% of class III velocities in the front quarter of the chest which represents 11% of the reconstructed volume) are found in the front part of the chest.

Table 1 Marble damage classes defined by Köhler [12] (after *Weiss et al. (2002)*)

Damage class	Ultrasonic pulse velocity (m/s)	Marble condition
0	> 5,000	Fresh
I	3,000 – 5,000	Increasingly porous
II	2,000 – 3,000	Granular disintegration
III	1,500 – 2,000	Fragile
IV	< 1,500	Crumbling rock

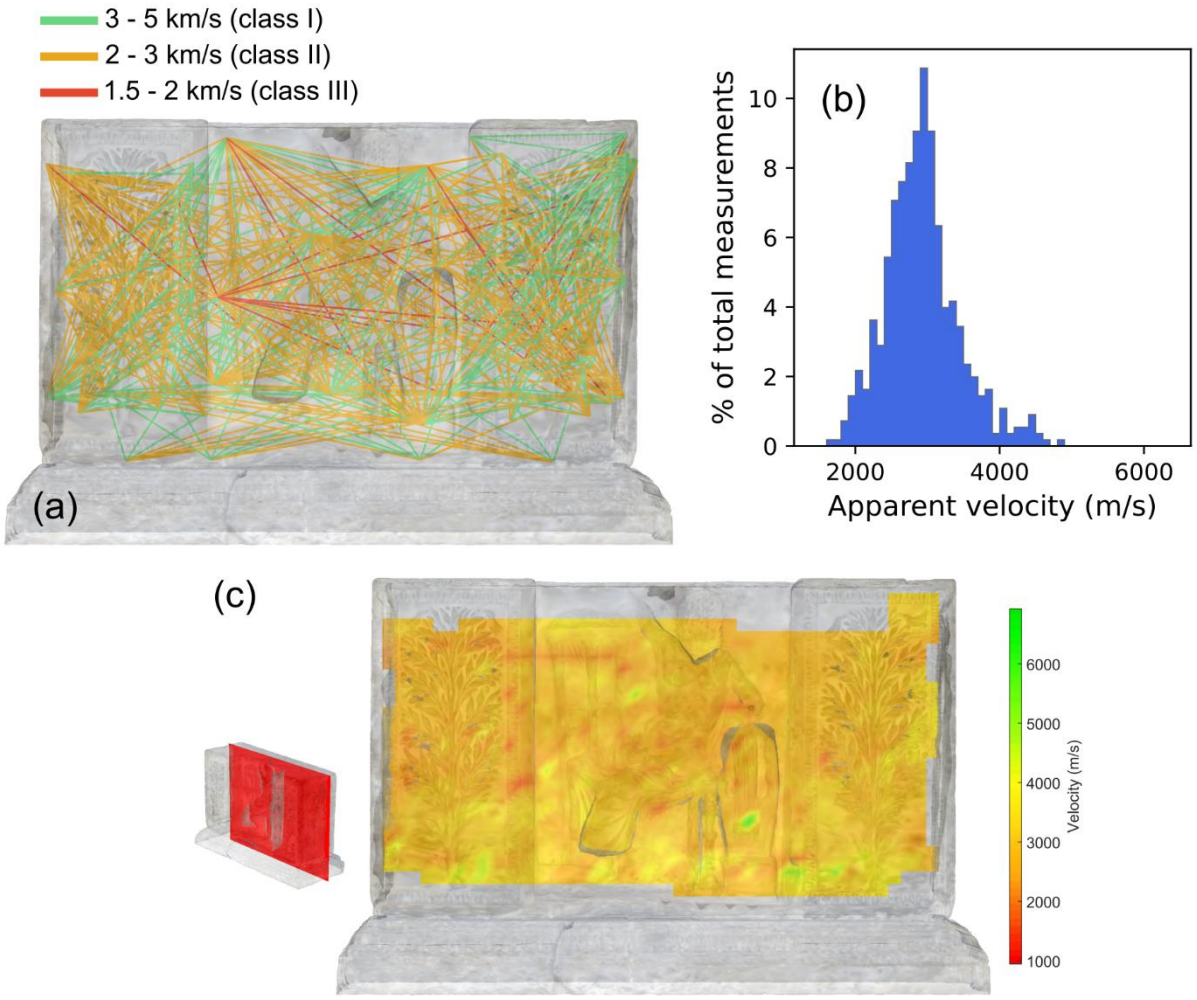

Fig. 4 (Color online) Tomography results for the Apollo altar. (a) Apparent propagation velocities classified according to Köhler damage classes (Table 1). (b) Histogram of the apparent propagation velocities. (c) Slice in the 3D imaging of the propagation velocity. The slice position is indicated by a red plan.

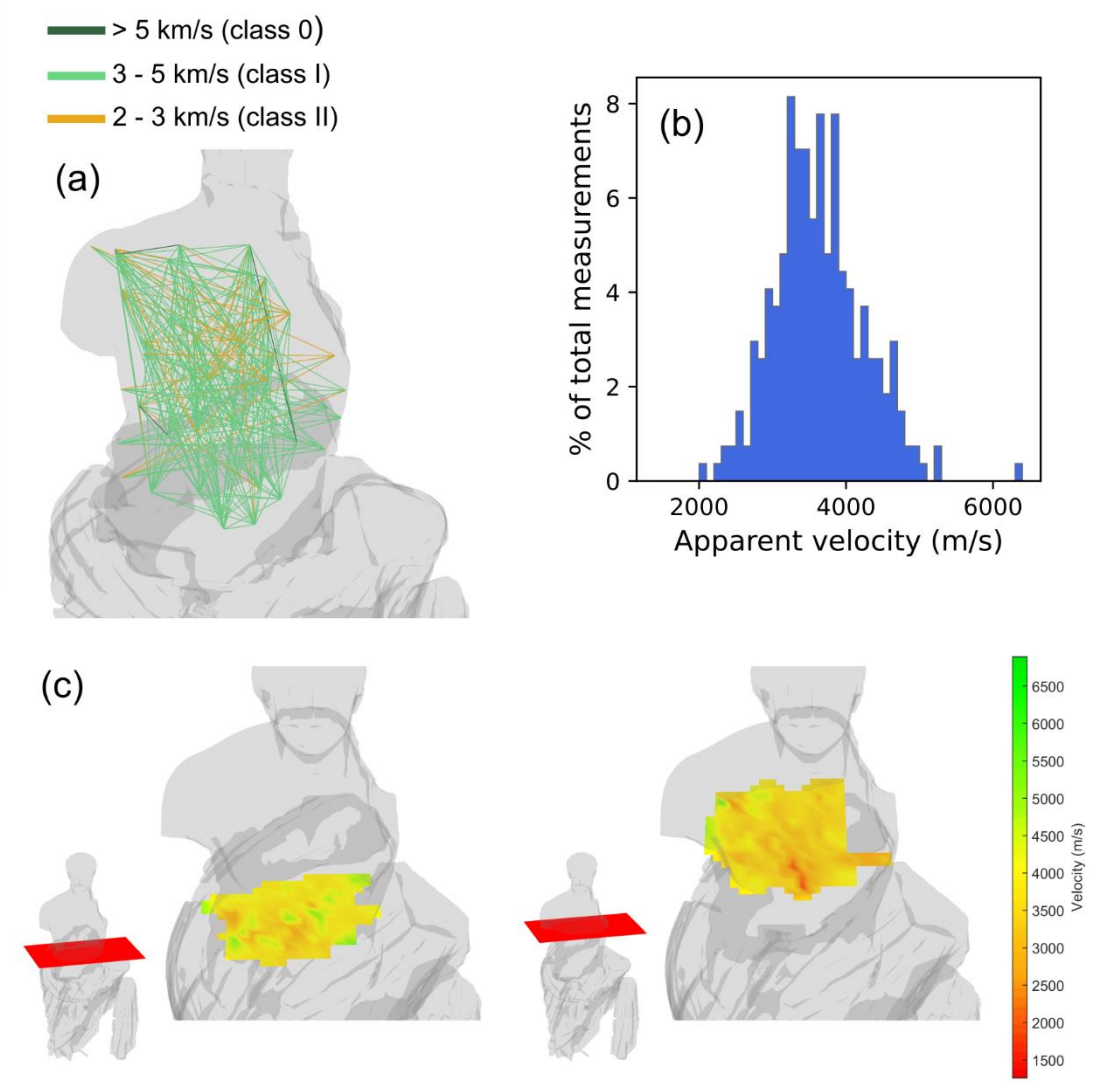

Fig. 5 (Color online) Tomography results for the Augustus statue. (a) Apparent propagation velocities classified according to Köhler damage classes (Table 1). (b) Histogram of the apparent propagation velocities. (c) Slices in the 3D imaging of the propagation velocity, in the lower and upper parts. The slice positions are indicated by red plans.

4.2.Crack depth measurement

Depth profiles were estimated for the Apollo altar cracks by evaluating their depth at different points along their length. The deduced crack geometries are schematized in Fig. 6 (a, b). The circle points correspond to the experimental depth measurements. The depth measurement data can be found in the Supplementary Material. The first and last data points were measured directly on the altar surface where the cracks emerge. The first three experimental data of the left-side crack and all the experimental data of the right-side crack were fitted to polynomial laws (dashed line in Fig. 6) to propose an estimation of the general crack depth profiles. The detection limit of the technique is evidenced in grey. The estimated depth profile for the right-side crack has an asymmetrical bell shape with local extrema reached at the altar front and back sides and a shallower portion of the crack in the middle width of the altar. The left-side crack is very superficial (probably shallower than 3 cm), except at the very front of the altar. The relationship between the time of flight and the distance was always linear for this crack, except at the first measurement point.

One objective of the acoustic tomography was to estimate the extent of the cracks visible at Apollo altar surface. At the theater destruction in the 5th century, the altar must have been damaged and the differences in thickness in the block must have played a role in creating these cracks. Fig. 6 (c) shows a velocity cartography in the crack zones at 12 cm from the altar top surface. This is the nearest reconstructed cartography to the altar top. The crack profiles at the surface are indicated by the red solid lines. This cartography can be compared to the crack depth estimations. According to the estimated depth profiles, at 12 cm from the top surface both cracks should be present at the front of the altar. However, the front part of the right-side crack coincides with a high velocity zone on the velocity cartography and the velocity in the zone of the left-side crack is very uniform.

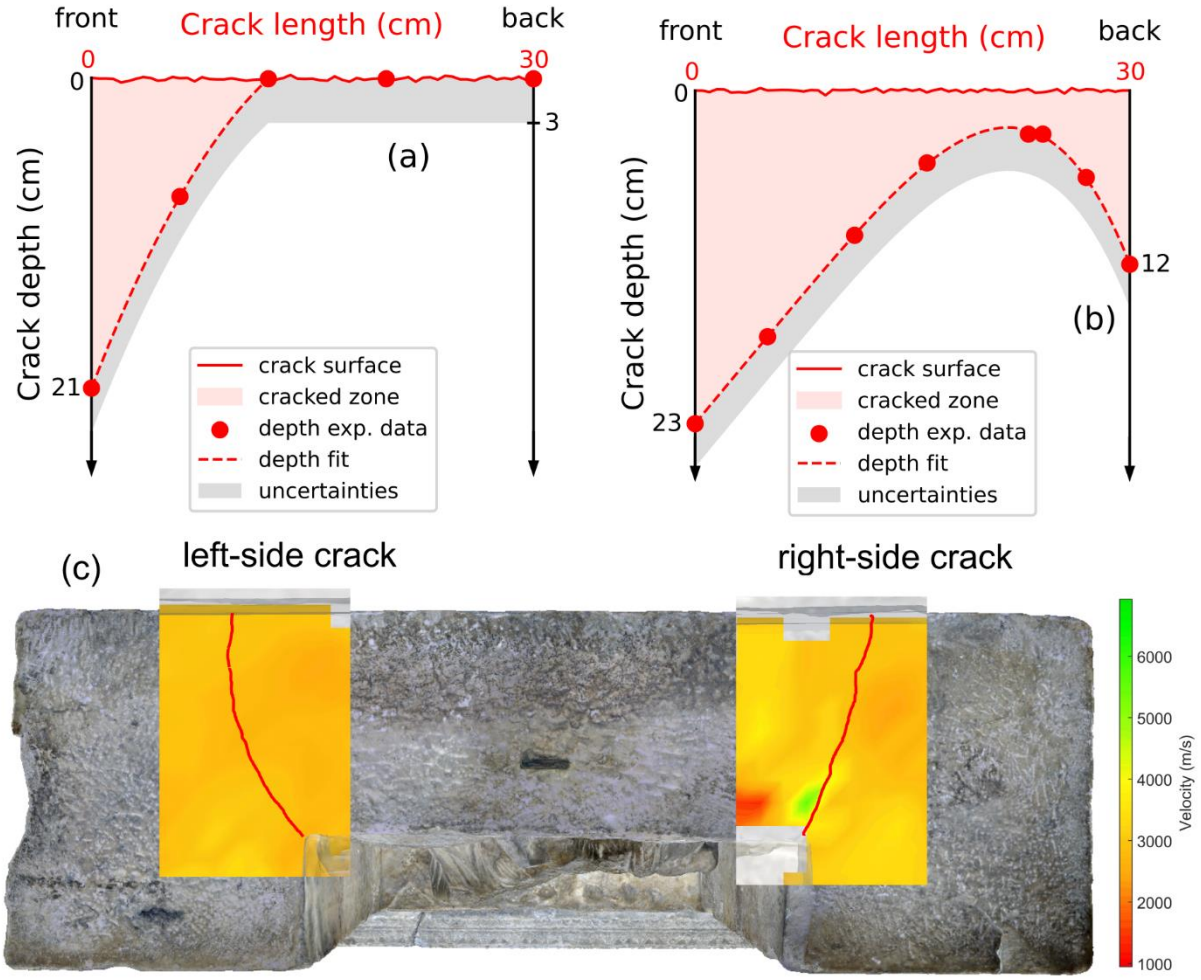

Fig. 6 (Color online) Apollo altar cracks. (a) Left side and (b) right side crack depth profiles estimated with several punctual measurements along the crack length. Circle data points correspond to experimental depth measurements, the dashed lines to polynomial fits of the experimental depths, the red zones to the cracked zones, the grey zones to uncertainties. (c) Velocity cartography in the crack zones of the Apollo altar at 12 cm below the top surface. The crack profiles at the surface are indicated by red solid lines.

5. Discussion

The degradation state of both sculptures is discussed based on the results of apparent propagation velocity, 3D imaging of propagation velocity, and crack depth measurements.

5.1. Global cohesion and areas of weakness

The apparent velocity results for both objects show that they display an acceptable cohesion state. Indeed, none of the global velocities in both sculptures belongs to damage class IV (Table 1) and only 14 measurements out of 560 (3%) in the Apollo altar belong to damage class III. Besides, the average apparent velocity value lies in damage class I for the statue and in the limit between damage classes I and II for the altar.

The apparent velocity results highlight that the Augustus statue exhibits a better conservation state than the Apollo altar. Indeed, the global apparent velocities in the statue have a higher average value, some belong to damage class 0 and none belongs to damage classes III and IV. These observations corroborate the outer visual inspections: the numerous cracks on Augustus' chest seemed superficial, whereas the two cracks crossing the altar from back to front seemed deeper and more worrying. The global worse cohesion state of the altar is in agreement with the sculpture locations in the Roman theater. Indeed, both front sides were facing east and could thus be exposed to direct sun radiations and rain. However, the statue was partially protected from insolation and rain by the *scaenae frons* and, possibly, by an awning, while the altar was much less protected and was fully exposed to rain.

Regarding weaker areas inside the two sculpted objects, the 3D velocity image of the Apollo altar indicates that the weakest zones of the sculpture are located at its back. This location is not the most exposed to weather conditions. However, the back was against the *pulpitum* wall. Therefore, this zone could have been damper than other altar parts as it was confined against the wall, with also possible capillary rises from the ground. Higher humidity levels could have thus induced more degradation in the altar back.

The 3D velocity image slices showed that the upper and front parts of Augustus' chest contain more low velocity values than the lower and back parts. Weaker zones in the upper part of the chest could be explained by the presence of a thick vein and of areas of breakage (left arm and head) in this area. Besides, the front part of the statue was more subjected to weather conditions than the back which was protected by a niche in the *scaenae frons*. In addition, the small cracks and circling vein on the front side of Augustus statue could contribute to a lesser cohesion in that part. The cracks are likely the result of a greater exposure to weathering and could be responsible for more damage as they made possible a deeper water penetration inside the marble.

Therefore, this approach coupling acoustic tomography to photogrammetry allowed investigating the inner degradation state of Carrara marble sculptures. Tomography has provided 3D images of the velocity that are physically consistent with ultrasonic pulse velocity values generally found in marble. The results also agree with the original hypotheses made on the global cohesion state of each sculpture according to their location in the Roman theater of Arles.

5.2. Crack depths

As shown by the results presented in section 4.2, the presence of both cracks cannot be correlated to the variations of the reconstructed local propagation velocities (Fig. 6). This lack of correlation may be due to the acquisition, reconstruction or interpolation procedures that tend to average the velocity values and could erase the effects of very local defects, or it could indicate that the cracks do not significantly impact the mechanical integrity of the altar.

The right-side crack was the most worrying for the curators. They feared that this crack had propagated across the entire height of the altar and that the right part would break away from the rest of the altar if it were moved. The estimated profiles (Fig. 6 (a , b)) for both cracks highlight that the right-side crack is indeed the most worrying one. However, they also show that this crack has not yet spread across the entire altar height. Therefore, the altar parts on either side of the crack still hold together. Nevertheless, moving the altar could increase the crack propagation and result in fracture. Therefore, the altar should not be moved without conservation operations. In the meantime, the risk associated with such displacements could be evaluated by conducting numerical simulations of the crack mechanical behavior in different displacement situations.

6. Conclusions

The degradation state of two Carrara marble sculptures from the Roman theater of Arles was investigated with a non-destructive diagnosis technique coupling acoustic tomography with photogrammetry to reconstruct a 3D imaging of the sculpture mechanical state. To overcome the difficulties imposed by the complex geometries of these sculptures, the 3D photogrammetric models were directly projected onto the sculptures during measurement campaigns to locate transducer positions. This way of implementing acoustic tomography offers an alternative method for locating transducers that avoids sticking markers on sculpture surfaces.

The results showed different degradation degrees in the two sculptures. Overall, their degradation degree coincides with their degree of exposure to weather conditions in the Roman theater. Therefore, these results once more highlight the significant sensitivity of marble to weather conditions and the difficulty of preserving this material from weathering.

Besides, the results also revealed that the most worrying crack of the Apollo altar has not yet propagated across its entire height. Contrary to what the curators feared, the middle and right lateral parts of the altar still hold together. These results emphasize the ability of non-destructive acoustic techniques to answer specific conservation issues and to be decision-support tools for curators. Nevertheless, the altar should not be moved unless conservation operations or numerical simulations of the crack behavior are conducted as its displacement could enhance crack propagation and induce mechanical fracture.

Acoustic tomography of stone sculptures could be further developed in future work. Here, crack depth had to be evaluated with another technique. The use of higher frequency transducers could bring more resolution and allow overcoming this limit. As a perspective, following the same methodology, ultrasound attenuation could be measured in addition to ultrasound propagation velocity, using a non-contact laser vibrometer for ultrasound reception. Indeed, the absence of contact (thus coupling interface) would allow reliable amplitude measurements which would provide a 3D attenuation map [19]. The technique could also become fully contactless by using a pulsed laser for ultrasonic emission and a vibrometer for reception.

Competing interests statement

The authors declare that they have no known competing financial interests or personal relationships that could have appeared to influence the work reported in this paper.

Funding sources

This work benefited from State aids managed by the Agence Nationale de la Recherche (French National Research Agency) under the investment for the future program integrated into France 2030, bearing the references ANR-17-EURE-0021 Ecole Universitaire de Recherche Paris Seine – Foundation for Cultural Heritage Sciences and ANR 21-ESRE-0050 EquipEX+ ESPADON.

Data statement

Data will be made available on request, except for the 3D models which belong to the Departmental Museum of Ancient Arles.

Acknowledgements

Authors wish to thank Alain Charron and Soizic Toussaint from the Departmental Museum of Ancient Arles for authorizing the authors to work on sculptures from the museum collection. Authors also thank Alain Charron for his proofreading of the manuscript and for the precisions he gave to the authors about the architecture and history of the Roman theater of Arles and about the precise locations and exposures of the two studied sculptures.

References

[1] ICOMOS-ISCS, Illustrated glossary on stone deterioration patterns - Glossaire illustré sur les formes d'altération de la pierre, Paris, 2008.
[2] P. Marini, R. Bellopede, The Influence of the Climatic Factors on the Decay of Marbles: an Experimental Study, American J. of Environmental Sciences 3 (2007) 143–150. https://doi.org/10.3844/ajessp.2007.143.150.
[3] S. Siegesmund, K. Ullemeyer, T. Weiss, E.K. Tschegg, Physical weathering of marbles caused by anisotropic thermal expansion, International Journal of Earth Sciences 89 (2000) 170–182. https://doi.org/10.1007/s005310050324.
[4] S. Siegesmund, J. Ruedrich, A. Koch, Marble bowing: comparative studies of three different public building facades, Environ Geol 56 (2008) 473–494. https://doi.org/10.1007/s00254-008-1307-z.
[5] K. Malaga, J.E. Lindqvist, B. Schouenborg, Experimental study on the variation in porosity of marble as a function of temperature, Geological Society, London, Special Publications 205 (2002) 81–88. https://doi.org/10.1144/GSL.SP.2002.205.01.07.
[6] A. Koch, S. Siegesmund, The combined effect of moisture and temperature on the anomalous expansion behaviour of marble, Env Geol 46 (2004). https://doi.org/10.1007/s00254-004-1037-9.
[7] A. Luque, E. Ruiz-Agudo, G. Cultrone, E. Sebastián, S. Siegesmund, Direct observation of microcrack development in marble caused by thermal weathering, Environ Earth Sci 62 (2011) 1375–1386. https://doi.org/10.1007/s12665-010-0624-1.
[8] B. Grelk, P. Goltermann, B. Schouenborg, A. Koch, L. Alneas, The laboratory testing of potential bowing and expansion of marble, in: Proceedings of the International Conference on Dimension Stone, Taylor & Francis Group plc, A.A. Balkerma Publische, Prague, Czech Republic, 2004: pp. 253–259.
[9] M.-L. Chavazas, P. Bromblet, J. Berthonneau, J. Hénin, C. Payan, Progressive thermal decohesion in Carrara marble monitored with nonlinear resonant ultrasound spectroscopy, Bull Eng Geol Environ 83 (2024). https://doi.org/10.1007/s10064-024-03875-8.
[10] M.-L. Chavazas, P. Bromblet, J. Berthonneau, J. Hénin, C. Payan, Impact of relative humidity variations on Carrara marble mechanical properties investigated by nonlinear resonant ultrasound spectroscopy, Construction and Building Materials 431 (2024) 136529. https://doi.org/10.1016/j.conbuildmat.2024.136529.
[11] T. Weiss, P.N.J. Rasolofosaon, S. Siegesmund, Ultrasonic wave velocities as a diagnostic tool for the quality assessment of marble, Geological Society, London, Special Publications 205 (2002) 149–164. https://doi.org/10.1144/GSL.SP.2002.205.01.12.
[12] W. Köhler, Untersuchungen zu Verwitterungsvorgängen an Carrara-Marmor in Potsdam-Sanssouci, Berichte Zu Forschung Und Praxis Der Denkmalpflege in Deutschland, Steinschäden-Steinkonservierung 2 (1991) 50–53.

[13] J. Ruedrich, C. Knell, J. Enseleit, Y. Rieffel, S. Siegesmund, Stability assessment of marble statuaries of the Schlossbrücke (Berlin, Germany) based on rock strength measurements and ultrasonic wave velocities, Environ Earth Sci 69 (2013) 1451–1469. https://doi.org/10.1007/s12665-013-2246-x.
[14] P. Capizzi, P.L. Cosentino, Electromagnetic and ultrasonic investigations on a Roman marble slab, J. Geophys. Eng. 8 (2011) S117–S125. https://doi.org/10.1088/1742-2132/8/3/S11.
[15] L. Sambuelli, G. Bohm, P. Capizzi, E. Cardarelli, P. Cosentino, Comparison between GPR measurements and ultrasonic tomography with different inversion algorithms: an application to the base of an ancient Egyptian sculpture, Journal of Geophysics and Engineering 8 (2011) S106–S116. https://doi.org/10.1088/1742-2132/8/3/S10.
[16] S. Fais, G. Casula, F. Cuccuru, P. Ligas, M.G. Bianchi, An innovative methodology for the non-destructive diagnosis of architectural elements of ancient historical buildings, Sci Rep 8 (2018) 4334. https://doi.org/10.1038/s41598-018-22601-5.
[17] T. Cavaleri, S. Legnaioli, F. Lozar, C. Comina, F. Poole, C. Pelosi, A. Spoladore, D. Castelli, V. Palleschi, A Multi-Analytical Study of an Ancient Egyptian Limestone Stele for Knowledge and Conservation Purposes: Recovering Hieroglyphs and Figurative Details by Image Analysis, Heritage 4 (2021) 1193–1207. https://doi.org/10.3390/heritage4030066.
[18] E. Grinzato, S. Marinetti, P.G. Bison, M. Concas, S. Fais, Comparison of ultrasonic velocity and IR thermography for the characterisation of stones, Infrared Physics & Technology 46 (2004) 63–68. https://doi.org/10.1016/j.infrared.2004.03.009.
[19] Q. Vu, C. Payan, E. Debieu, P. Lasaygues, M. Bagnéris, A. Pamart, F. Cherblanc, P. Bromblet, Ultrasonic imaging of antique statue combining laser vibrometry and photogrammetry, (2018). https://hal.science/hal-01883674v1.
[20] L. Sambuelli, G. Böhm, C. Colombero, A. Filipello, Photogrammetry and 3-D Ultrasonic Tomography to Estimate the Integrity of Two Sculptures of the Egyptian Museum of Turin, in: European Association of Geoscientists & Engineers, Turin, Italy, 2015. https://doi.org/10.3997/2214-4609.201413675.
[21] V. Di Pietra, E. Donadio, D. Picchi, L. Sambuelli, A. Spanò, MULTI-SOURCE 3D MODELS SUPPORTING ULTRASONIC TEST TO INVESTIGATE AN EGYPTIAN SCULPTURE OF THE ARCHAEOLOGICAL MUSEUM IN BOLOGNA, Int. Arch. Photogramm. Remote Sens. Spatial Inf. Sci. XLII-2/W3 (2017) 259–266. https://doi.org/10.5194/isprs-archives-XLII-2-W3-259-2017.
[22] F. Vagnon, C. Comina, M.C. Canepa, A. Bovero, G. Giraudo, Experiences and preliminary results of geophysical methods on historical statues, IOP Conf. Ser.: Earth Environ. Sci. 1124 (2023) 012132. https://doi.org/10.1088/1755-1315/1124/1/012132.
[23] C. Colombero, P. Dabove, N. Grasso, F. Khosro Anjom, F. Pace, S. Aicardi, Microgeophysics and geomatics data integration reveals the internal fracturing conditions of the statue of Ramses II (Museo Egizio, Torino, Italy), Sci Rep 12 (2022) 9933. https://doi.org/10.1038/s41598-022-14300-z.
[24] P. Capizzi, P.L. Cosentino, S. Schiavone, Some tests of 3D ultrasonic traveltime tomography on the Eleonora d'Aragona statue (F. Laurana, 1468), Journal of Applied Geophysics 91 (2013) 14–20. https://doi.org/10.1016/j.jappgeo.2013.01.012.
[25] E. Cardarelli, R. De Nardis, Seismic refraction, isotropic anisotropic seismic tomography on an ancient monument (Antonino and Faustina temple AD 141), Geophysical Prospecting 49 (2001) 228–240. https://doi.org/10.1046/j.1365-2478.2001.00251.x.
[26] M. Bagnéris, F. Cherblanc, P. Bromblet, E. Gattet, L. Gügi, N. Nony, V. Mercurio, A. Pamart, A complete methodology for the mechanical diagnosis of statue provided by innovative uses of 3D model. Application to the imperial marble statue of Alba-la-Romaine (France), Journal of Cultural Heritage 28 (2017) 109–116. https://doi.org/10.1016/j.culher.2017.05.002.
[27] J. Zhang, K. Khoshelham, 3D reconstruction of internal wood decay using photogrammetry and sonic tomography, The Photogrammetric Record 35 (2020) 357–374. https://doi.org/10.1111/phor.12328.
[28] M. Puxeddu, F. Cuccuru, S. Fais, G. Casula, M.G. Bianchi, 3D Imaging of CRP and Ultrasonic Tomography to Detect Decay in a Living Adult Holm Oak (Quercus ilex L.) in Sardinia (Italy), Applied Sciences 11 (2021) 1199. https://doi.org/10.3390/app11031199.

[29] Collectif, Musée de l'Arles antique, catalogue, Actes Sud, 1996.
[30] Climate and annual weather averages in Arles, France, (n.d.). https://fr.weatherspark.com/y/50260/M%C3%A9t%C3%A9o-moyenne-%C3%A0-Arles-France-tout-au-long-de-l'ann%C3%A9e (accessed September 3, 2024).
[31] C. Carrier, Sculptures augustéennes du théâtre d'Arles, ran 38 (2005) 365–396. https://doi.org/10.3406/ran.2005.1164.
[32] R. Altindag, Correlation between P-wave velocity and some mechanical properties for sedimentary rocks, J. S. Afr. Inst. Min. Metall. 112 (2012).
[33] S. Siegesmund, J. Menningen, V. Shushakova, Marble decay: towards a measure of marble degradation based on ultrasonic wave velocities and thermal expansion data, Environ Earth Sci 80 (2021) 395. https://doi.org/10.1007/s12665-021-09654-y.
[34] S. Toussaint, La numérisation au musée départemental Arles antique: Une valorisation des collections archéologiques, Nda (2017) 32–38. https://doi.org/10.4000/nda.3750.
[35] P.C. Hansen, M. Saxild-Hansen, AIR Tools — A MATLAB package of algebraic iterative reconstruction methods, Journal of Computational and Applied Mathematics 236 (2012) 2167–2178. https://doi.org/10.1016/j.cam.2011.09.039.
[36] P.C. Hansen, J.S. Jørgensen, AIR Tools II: algebraic iterative reconstruction methods, improved implementation, Numer Algor 79 (2018) 107–137. https://doi.org/10.1007/s11075-017-0430-x.
[37] B. Abayowa, display_obj, (2008). https://www.mathworks.com/matlabcentral/fileexchange/20307-display_obj (accessed November 3, 2023).
[38] B. Abayowa, readObj, (2008). https://www.mathworks.com/matlabcentral/fileexchange/18957-readobj (accessed November 3, 2023).
[39] A. Luthfian, dispObj, (2018). https://www.mathworks.com/matlabcentral/fileexchange/66275-david-laserscanner-wavefront-obj-file-reader-plotter-volume-and-surface-area-calculator (accessed May 23, 2024).
[40] A. Ahmad, M. Pamplona, S. Simon, Ultrasonic testing for the investigation and characterization of stone – a non-destructive and transportable tool, Studies in Conservation 54 (2009) 43–53. https://doi.org/10.1179/sic.2009.54.Supplement-1.43.
[41] G. Pascale, A. Lolli, Crack assessment in marble sculptures using ultrasonic measurements: Laboratory tests and application on the statue of David by Michelangelo, Journal of Cultural Heritage 16 (2015) 813–821. https://doi.org/10.1016/j.culher.2015.02.005.

Supplementary material

A. Emitter and receiver positions in the Apollo altar and the Augustus statue

B. Histograms of the propagation velocities in the Apollo altar and the Augustus statue

C. Propagation velocities classified by damage classes in different parts of the Apollo altar and the Augustus statue

D. Crack depth data from the Apollo altar

A. Emitter and receiver positions in the Apollo altar and the Augustus statue

The following figures present the positions of the emitter and the receiver during the measurement campaign on the Apollo altar and the Augustus statue.

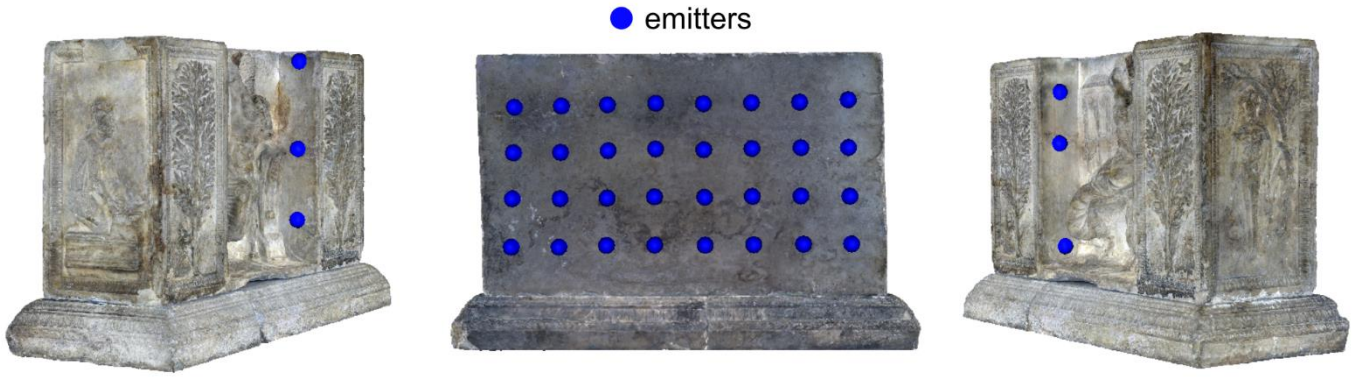

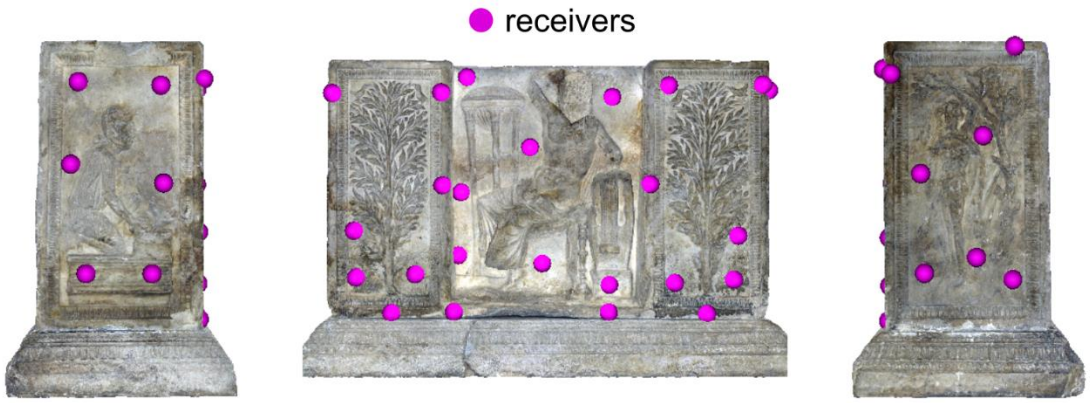

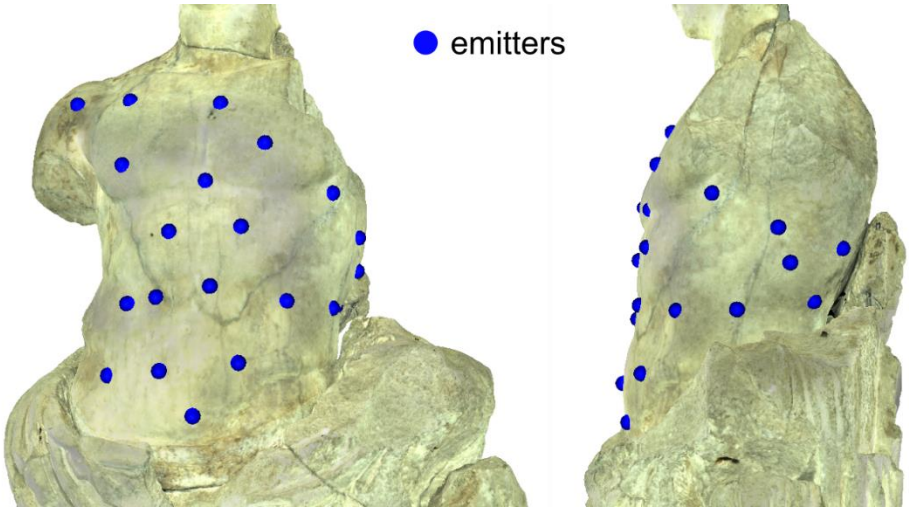

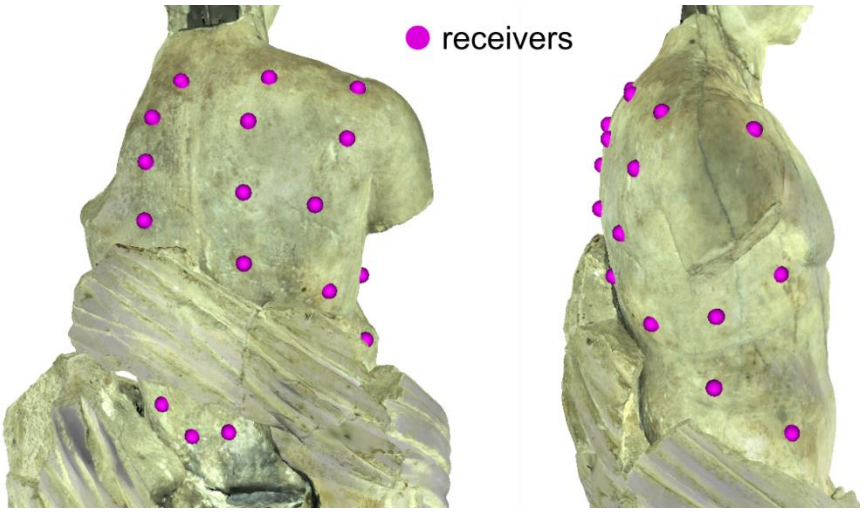
receivers

B. Histograms of the propagation velocities in the Apollo altar and the Augustus statue

The following histograms represent the propagation velocities in the Apollo altar and the Augustus statue.
Fig. (a) corresponds to the apparent propagation velocities measured experimentally on both sculptures. The apparent velocities were calculated from the measured times of flight and the distances between each emitter and receiver assuming a straight path of ultrasound in the sculptures.

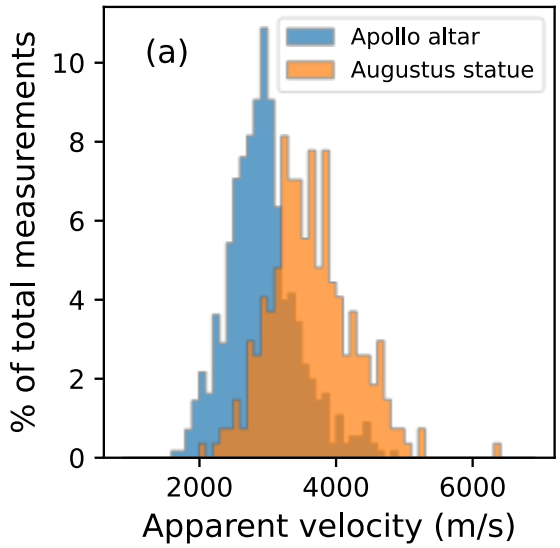

Fig. (b) and (c) correspond to propagation velocities calculated thanks to the SIRT (Simultaneous Iterative Reconstruction Techniques) algorithm. Fig. (b) corresponds to the local velocities in each voxel in which the sculptures were virtually discretized for the inversion procedure. These velocities are directly returned by the SIRT algorithm. From these local velocity values, the global ultrasonic pulse velocities (UPV) were recalculated and their histogram is presented in Fig. (c). Fig. (a) and (c) show a good agreement in the general shape of the histograms between the experimental and recalculated UPV.

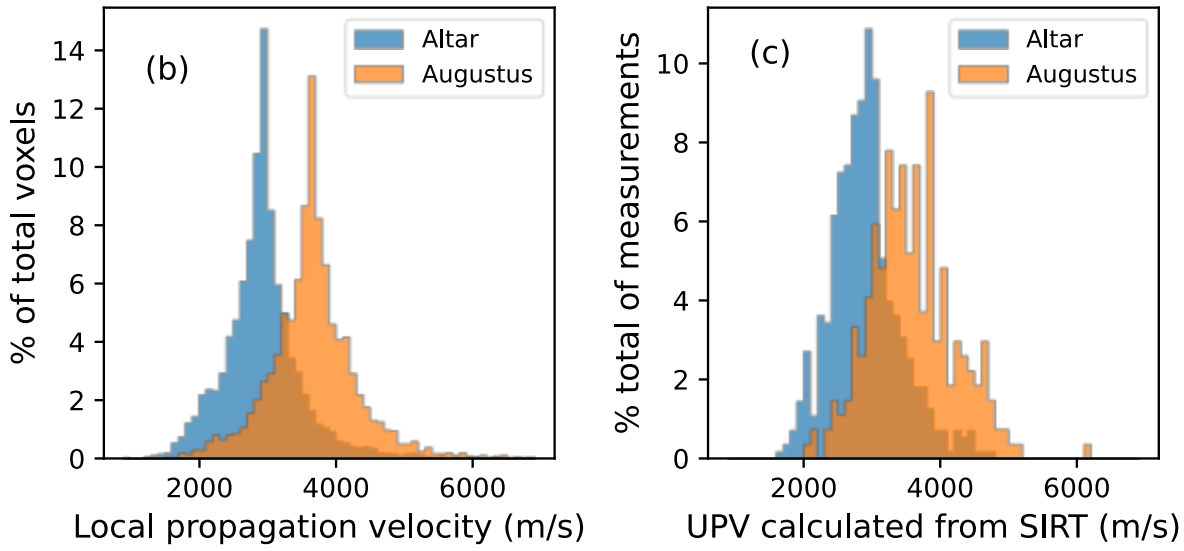

C. Propagation velocities classified by damage classes in different parts of the Apollo altar and the Augustus statue

In Table 2 and Table 3, the propagation velocities in the Apollo altar and the Augustus statue, respectively, are classified according to marble damage classes defined by Köhler (1991).
Different zones of the sculptures are considered. The "Entire altar/bust – Exp. UPV" columns correspond to the global apparent velocities measured experimentally. The "Entire altar/bust – SIRT" columns correspond to the local propagation velocities calculated by SIRT. All the columns focusing on portions of the sculptures correspond to local velocities calculated by SIRT. The percentages of volume correspond to percentages of the volume taken into account for the SIRT algorithm, not the entire sculpture volume. The "% by class" columns correspond to the repartition by damage class of the propagation velocities in the considered zone. The "% of entire class" columns correspond to the proportion of the propagation velocities of a given classes in this zone, as a fraction of the entire class.

Table 2 Propagation velocities in the Apollo altar classified by damage classes.

Class	Entire altar – Exp. UPV		Entire altar - SIRT		Back third = 41% vol.			Left jamb = 29% vol.			Right jamb = 29% vol.			Top half = 47% vol.			Back half = 60% vol.		
	Nb of UPV	% by class	Nb of voxels	% by class	Nb of voxels	% by class	% of entire class	Nb of voxels	% by class	% of entire class	Nb of voxels	% by class	% of entire class	Nb of voxels	% by class	% of entire class	Nb of voxels	% by class	% of entire class
0	0	0	76	1	34	1	45	23	1	30	19	0.9	25	14	0.4	18	43	1	57
I	215	39	2567	36	1045	36	41	714	34	28	734	36	29	1080	33	42	1497	35	58
II	323	59	4076	58	1620	56	40	1241	60	30	1203	59	30	2064	62	51	2471	58	61
III	14	3	296	4	170	6	57	90	4	30	88	4	30	146	4	49	211	5	71
IV	0	0	26	0.4	15	0.5	57	9	0.4	35	5	0.2	19	16	0.5	62	15	0.4	58

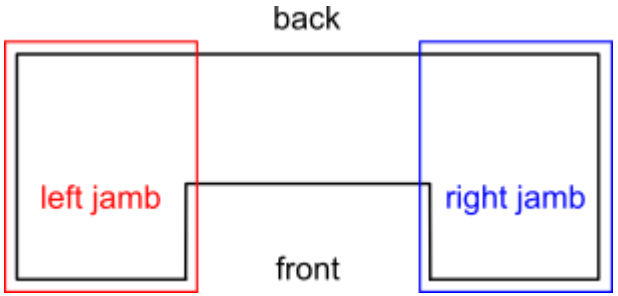

◄ Apollo altar zones

Table 3 Propagation velocities in the Augustus statue classified by damage classes.

Class	Entire bust – Exp. UPV		Entire bust – SIRT		Front quarter = 12% vol.			Front half = 47% vol.			Top half = 57% vol.			Right half = 47% vol.		
	Nb of UPV	% by class	Nb of voxels	% by class	Nb of voxels	% by class	% of entire class	Nb of voxels	% by class	% of entire class	Nb of voxels	% by class	% of entire class	Nb of voxels	% by class	% of entire class
0	4	1	115	3	20	5	17	53	3	46	51	3	44	33	2	29
I	228	84	2979	84	341	81	11	1375	82	46	1653	82	55	1418	86	48
II	38	14	404	11	55	13	14	238	14	59	304	15	75	191	12	47
III	0	0	27	0.8	6	1	22	15	0.9	56	10	0.5	37	13	0.8	48
IV	0	0	1	0.03	1	0.2	100	1	0.06	100	1	0.05	100	1	0.06	100

D. Crack depth data from the Apollo altar

Table 4 Crack depth measurements on the Apollo altar. Measurement points are located in the figures presented below.

Left-side crack (Fig. (a))		
Measurement point	Distance along crack from altar front	Measured depth
Altar front	0 cm	21 cm[(a)]
1	6 cm	8 cm
2	12 cm	0 cm[(b)]
3	20 cm	0 cm[(b)]
Altar back	30 cm	0 cm[(c)]
Right-side crack (Fig. (b) and (c))		
Measurement point	Distance along crack from altar front (or top for points no. 5 and 6)	Measured depth
Altar front	0 cm	23 cm[(a)]
1	5 cm	17 cm
2	11 cm	10 cm
3	16 cm	5 cm
4	23 cm	3 cm
Altar back	30 cm	12 cm[(a)]
5	3 cm (from altar top)	6 cm
6	6 cm (from altar top)	3 cm

(a) measured with a tape measure along crack emergence at front and back sides

(b) uncertainty due to crack detection limit: 3 cm

(c) no crack emergence at the back of the altar